Biotechnology Reports 47 (2025) e00904

Contents lists available at ScienceDirect

Biotechnology Reports

journal homepage: www.elsevier.com/locate/btre

Investigation and optimization of DNA isolation efficiency using ferrite-based magnetic nanoparticles

Tímea B. Gerzsenyi [a,b], Ágnes M. Ilosvai [a,b], Ferenc Kristály [c], Lajos Daróczi [d], Michael C. Owen [a], Béla Viskolcz [a,b], László Vanyorek [b], Emma Szőri-Dorogházi [b,*]

[a] Higher Education and Industrial Cooperation Centre, University of Miskolc, 3515 Miskolc, Hungary
[b] Institute of Chemistry, University of Miskolc, 3515 Miskolc, Hungary
[c] Institute of Mineralogy and Geology, University of Miskolc, 3515 Miskolc, Hungary
[d] Department of Solid State Physics, University of Debrecen, 4010 Debrecen, Hungary

ARTICLE INFO

Keywords:
DNA isolation
bacterial DNA
Magnetic nanoparticles
Cost-effectiveness

ABSTRACT

DNA isolation is a crucial step in many molecular biological applications for diagnostic and research purposes, like detection of infectious diseases or gene expression studies. However, due to the requirement of toxic reagents in traditional procedures and the high expenses of commercial kits, the use of magnetic MNP-based DNA isolation is becoming more widespread. In this study, different ferrite containing MNPs ($MnFe_2O_4$, $MnFe_2O_4$-NH_2, $MgFe_2O_4$, $MgFe_2O_4$-NH_2 $NiFe_2O_4$, $NiFe_2O_4$-NH_2) are examined and compared in their pDNA isolation efficiency. Among the tested nanoparticles, we document the use of $NiFe_2O_4$ and its amine-functionalized form for the first time. Three protocols for the isolation of pDNA are optimized for each type of nanoparticle and the best protocol is selected based on the quantity, quality and integrity of the extracted DNA. Plasmid samples extracted with the MNPs are transformed into competent bacterial cells and further tests are performed to recover genomic DNA from bacterial cells, leading to the development of another protocol. Bacteria-spiked blood serum samples are produced to extract DNA from a more complex biological matrix.

1. Introduction

Magnetic nanoparticles (MNPs) have garnered significant interest among researchers due to their good biocompatibility, tuneable surface chemistry, morphology and magnetic properties, which lead to their versatile applications across various technological fields [1]. A 2023 review highlights the rising economic relevance of nanotechnology, hence the use of MNPs, showing steady growth in global nanotech patents from 2000 to 2020 and an increasing ratio of nanotech contribution to nominal GDP [2]. Large-scale MNP production is considered low-risk, with costs typically recovered within the first year. A 2024 study reported a projected net present value (NPV) of USD 28,033,346 and a benefit-cost ratio of 2.07, indicating strong profitability and return on investment [3].

In recent years, MNPs have mainly been tested and utilized in medical diagnostics and treatments, however a growing body of literature describes their potential uses in agriculture and environmental protection [4,5]. In a recent study, a MNP biosensor was developed using agricultural waste and modified through $MnFe_2O_4$ coprecipitation, then these nanoparticles were subsequently employed as adsorbents to effectively remove copper(II) ions from water, addressing the escalating health risks associated with their presence in drinking water [6]. On the other hand, manganese ferrite MNPs have been shown to be effective micronutrient fertilizers for wheat [7]. Further studies have highlighted the wider application of magnetic nanoparticles in wastewater treatment [8], as the mutagenic and carcinogenic crystal violet (CV) dye was effectively adsorbed onto the surface of nickel ferrite nanoparticles, achieving a removal efficiency of 95 % after just one hour of incubation [9].

Magnetic nanoparticles (e.g. $MnFe_2O_4$, $NiFe_2O_4$) with a lipid bilayer or encapsulated in a liposome, can serve as targeted drug carriers or hyperthermia agents in an important medical application. Using a magnetic field, these nanoparticles can deliver bound molecules to targeted cells [10,11]. Another medical implementation is magnetic resonance imaging (MRI). Ferrite based MNPs (e.g. $MnFe_2O_4$, $MgZnFe_2O_4$), particularly those with superparamagnetic properties, are highly suitable for MRI contrast agents. Their efficacy is further enhanced when they exhibit uniformity within a narrow size distribution at the

* Corresponding auithor.
E-mail address: emma.szori-doroghazi@uni-miskolc.hu (E. Szőri-Dorogházi).

https://doi.org/10.1016/j.btre.2025.e00904
Received 11 February 2025; Received in revised form 26 May 2025; Accepted 29 June 2025
Available online 30 June 2025

nanoscale [12–15]. Nanoparticles are also utilized in everyday life, for instance in food packaging that releases nanoscale antimicrobial compounds and antioxidants, thus extending the shelf life of food [16].

Given the great attention magnetic nanoparticles are receiving in the field of medicine, it is crucial to investigate their cytotoxicity. Antibacterial effects have also been investigated and proven on some modified ferrite-based nanoparticles, such as cobalt doped magnesium ferrite [17], however manganese ferrite seemed to not have any antibacterial or anti-fungal activity [18]. Previous studies on the cytotoxicity of magnesium ferrite have demonstrated varying levels of cell damage across different cell types, such as l-929 mouse aerola fibroblast cell lines. As the cytotoxicity of iron oxide nanoparticles has been linked to cellular uptake and reactive oxygen species production [19], this variability in cell damage may be attributed to the distinct free radical toxicity profiles of different cell types, with some cells exhibiting greater tolerance to the production and intracellular entry of free radicals compared to others [20–23]. Given the direct contact between nanoparticles and red blood cells during MRI examinations, a study was conducted to investigate the cytotoxic effects of nickel ferrite on human erythrocytes [24]. The presence of MNP was found to have a toxic effect on red blood cells by stimulating oxidative stress. However, when magnetic nanoparticles are used in separation methods to test extracted nucleic acids through downstream molecular biological techniques, cytotoxicity is not a concern. This is because MNPs only interact with the *in vitro* cell lysate, and do not make direct contact with the skin or bodily tissue of laboratory personnel [25].

Given the demonstrated suitability of certain ferrite-based magnetic nanoparticles for DNA isolation (e.g. cobalt ferrite [26], cobalt-zinc ferrite [27]), exploring and comparing the potential of other ferrite-based MNPs is the next logical step. Further characterizing the suitability of MNPs will expand the MNP toolkit available for researchers and enhance their flexibility to choose materials tailored to specific experimental conditions or specific biological samples. Additionally, identifying more magnetic nanoparticles suitable for DNA isolation could lead to optimized performance for diverse applications, fostering innovation in protocol development.

Extraction of DNA from crude biological samples can be generally classified into either fluid-phase or solid-phase methods [28]. Fluid-phase isolation requires the use of a phenol/chloroform mixture or cetyltrimethylammonium bromide (CTAB) and it typically includes centrifugation, precipitation and filtration steps. Solid-phase processes, such as the use of paramagnetic nanoparticles, offer significant advantages over the use of both commercially-available isolation kits and traditional DNA extraction methods, which require organic solvents. Separation techniques using MNPs cause minimal physical or chemical damage to nucleic acids and eliminate the need for laborious centrifugation and toxic reagents (e.g. phenol, chloroform) compared to traditional isolation methods. Furthermore, MNPs can be easily manipulated chemically or physically [29] and this kind of DNA extraction is highly suitable for automatization as well as up-scaling [30]. Additionally, as opposed to commercially-available DNA isolation kits, MNP-based extraction, such as the protocols described in this study are also relatively inexpensive [31] (Table 1).

In many molecular biological techniques that require isolated DNA, the quantity and quality of the applied DNA can be crucial to the success of the subsequent investigation. In one of our previous research articles we developed a plasmid DNA isolation protocol using manganese ferrite nanoparticles [25] and subsequently refined this protocol [33] for use with amine-functionalized magnesium ferrite MNPs. As a result, three distinct protocols have been established, each varying in two specific buffers: the binding buffer, which provides the conditions for DNA adsorption on the surface of MNPs, and the elution buffer, which facilitates the desorption process. In this work we have also tested the efficiency of the three protocols in combination with the following six magnetic nanoparticles: $MnFe_2O_4$, $MnFe_2O_4$-NH_2, $MgFe_2O_4$, $MgFe_2O_4$-NH_2 $NiFe_2O_4$, $NiFe_2O_4$-NH_2. We herein describe the use of a nickel ferrite MNP along with the amine-functionalized variant, in pDNA (plasmid DNA) isolation for the first time. In the second part of this study, we tested the most suitable and effective MNP for both bacterial genomic DNA (gDNA) isolation and pDNA extraction from a complex sample combining blood serum and bacterial cell culture.

Table 1
Material costs of the developed protocols, compared to traditional isolation [32] and commercially-available isolation kits. All of them were calculated based on their prices on the VWR website (https://hu.vwr.com/store) accessed in January 2025.

Name of protocol/kit		Price for 96 DNA isolations (EUR)
Developed MNP-based protocols	1. Tris–HCl	17.88
	2. PB	17.87
	3. Tris–HCl, NaCl	17.76
Traditional isolation		35.08
MNP-based isolation kits	Omega Bio-tek	120.92
	Zymo Research	168.33
Column-based isolation kits	Omega Bio-tek	631.89
	QIAGEN	1283.96

2. Materials and methods

2.1. Materials

Chemicals and materials used for the synthesis of magnetic nanoparticles, the establishment, growth and maintainance of cell cultures, DNA isolation steps and downstream molecular biological processes (DNA concentration and purity measurement, agarose gel electrophoresis, restriction digestion reactions, qPCR, bacterial transformation and preparation of bacteria-spiked blood serum sample) are listed by method in section *S1* of the *Supplementary Information* (*SI*).

2.2. Synthesis of magnetic nanoparticles

The non-functionalized magnetic nanoparticles were synthesized using an ultrasonic polyol method, whereas a solvothermal method was used to synthesize the amine-functionalized MNPs. For the polyol method, nitrate salts of transition metals ($Mn(NO_3)_2$ or $Ni(NO_3)_2$, 8 mmol) and $Fe(NO_3)_3$ (16 mmol) were dissolved in polyethylene glycol (PEG) and sonicated using an ultrasonic homogenizer for 3 min. This ultrasound treatment caused microbubble formation, which burst under high pressure [34], releasing localized thermal energy that triggered PEG to act as a reducing agent. This process led to the formation of metal hydroxide nanoparticles. To remove the PEG, the nanoparticles were heated to 300 °C for 3 h, converting the metal hydroxides into magnetizable spinel structures. Magnetism was used to isolate the MNPs.

In the solvothermal method that yielded the amine-functionalized magnetic nanoparticles, $Fe(NO_3)_3$ (2 mmol) and a transition metal nitrate ($Mn(NO_3)_2$ or $Ni(NO_3)_2$, 1 mmol) were dissolved in ethylene glycol and combined with a preheated sodium acetate solution. Ethanolamine (35 mL) was then added, and the mixture was refluxed at 200 °C for 12 h with continuous stirring. After cooling, the nanoparticles were collected by centrifugation, washed, and dispersed in distilled water. Detailed steps of the synthesis are shown in *S2.1* of the *SI*.

2.3. Physico-chemical characterization of the nanoparticles

High-resolution transmission electron microscopy (HRTEM) was employed to assess the size and morphology of the MNPs using a Talos F200X G2 electron microscope equipped with a field emission electron gun and a high-angle annular dark-field (HAADF) detector. MNP samples were dispersed in water, applied to copper grids, and imaged with a Ceta 16 Mpixel CMOS camera.

Phase identification and quantification of oxide forms were performed via X-ray diffraction (Bruker D8 diffractometer), while surface functional groups were analyzed with Fourier transform infrared spectroscopy (FTIR, Vertex 70) on pelletized samples with potassium bromide.

Magnetic characterization was conducted using a vibrating sample magnetometer, with magnetization measured at room temperature up to a field of 10,000 Oe.

These techniques provided comprehensive structural, surface and magnetic profiles for the synthesized nanoparticles. More detailed description of the MNP characterization and results can be found in the *Supplementary Information* (*S2.2*).

2.4. Preparation of bacterial cell suspensions

Bacterial cells were inoculated from LB agar plates to LB media and cultured in a shaking incubator for an overnight period at the temperature most suitable for the growth of each bacterial strain [35–38]. After culturing, the optical density (OD) of the cell suspensions was measured on 600 nm on NanoDrop™ One Microvolume UV–Vis spectrophotometer from Thermo Fisher Scientific (Waltham, MA, USA). The OD value is proportional to the cell concentration, indicating successful cell growth during overnight incubation with shaking.

2.5. Optimization of pDNA isolation using protocol 1 (Tris–HCl), protocol 2 (PB) and protocol 3 (Tris–HCl, NaCl)

The main steps of the isolation protocol developed previously [25] are summarized below, while Table 2 illustrates the exact buffers used in each of the three protocols.

Lysis *of Escherichia coli* bacterial cells was carried out by the precipitation of intracellular macromolecules (nucleic acids, proteins, lipids) at an alkaline pH (200 mM NaOH, 1 % SDS), and subsequently neutralizing the pH of the solution with 2.3 M CH_3COOK to renaturate the pDNA. Adsorption was achieved by adding MNPs dispersed in binding buffer to the pDNA solution (final concentration of the MNP dispersion was 10 mg/mL), and subsequently incubating the sample in a tube rotator for 10 min, before a magnetic stand was used to remove the supernatant without disturbing the pDNA-MNP complexes. Thereafter, the complexes were washed 3 times with a 20:80 mixture of aqueous 10 mM Tris–HCl and ethanol and dried at 37 °C. Desorption was achieved by adding the elution buffer and incubating each sample at 37 °C for 10 min. Finally, a magnetic stand was used to separate the MNPs from the isolated pDNA.

2.6. Evaluation criteria of the isolated pDNA

Each of the three protocols were utilized with six different nanoparticles ($MnFe_2O_4$, $MnFe_2O_4$-NH_2, $MgFe_2O_4$, $MgFe_2O_4$-NH_2 $NiFe_2O_4$, $NiFe_2O_4$-NH_2) to assess the ability of each of the eighteen combinations to isolate plasmid DNA. Five criteria were used to evaluate the protocol-MNP combinations: 1. the concentration of the extracted pDNA, 2. the purity of the extracted pDNA, 3. the resolution of isolated pDNA strands after agarose gel electrophoresis, 4. the fragmentation yield of pDNA following reactions with restriction endonucleases and 5. the integrity evaluation of the isolated pDNA with qPCR (quantitative polymerase chain reaction).

They are explained in further detail as follows:

Table 2
Composition of binding and elution buffers in the different protocols. Changes from Protocol 1 are marked in red (ø NaCl = no NaCl was used).

Isolation procedure	Binding buffer (adsorption)	Elution buffer (desorption)
Protocol 1 (Tris–HCl)	**2.5 M NaCl**, 10 mM Tris–HCl (pH 8.0), 1 mM EDTA, 20 % (w/v) PEG 6000, 0.05 % Tween 20	10 mM Tris–HCl (pH 7.0)
Protocol 2 (PB (Phosphate Buffer))	**2.5 M NaCl**, 10 mM Tris–HCl (pH 8.0), 1 mM EDTA, 20 % (w/v) PEG 6000, 0.05 % Tween 20	0.1 M K_3PO_4 (pH 8.0)
Protocol 3 (Tris–HCl, NaCl)	10 mM Tris–HCl (pH 8.0), 1 mM EDTA, 20 % (w/v) PEG 6000, 0.05 % Tween 20, **ø NaCl**	10 mM Tris–HCl (pH 7.0), **800 mM NaCl**

1. Concentration measurement of the extracted pDNA:

DNA concentration was measured using the NanoDrop™ One Microvolume UV–Vis spectrophotometer. The absorbance of the pDNA sample was measured at the specific wavelength of 260 nm (A_{260}). Based on the literature correlation that A_{260} = 1.0 corresponds to 50 μg of double-stranded DNA, the concentration of the sample can be calculated [39,40]. Commercially-available MNP-based pDNA isolation kit (Mag-Bind Ultra-Pure Plasmid DNA Kit, Omega Bio-tek) guarantees 10 μg/mL of the extracted pDNA (for high copy plasmids – 300–1000 copy/cell) [41]. Even though the pDNA isolated in this research (pBAD24) is a low copy plasmid with 10–20 molecules/cell, we set the threshold for the isolation to at least 10 μg/mL. This criterion was established because one of our objectives is to optimize the protocol to achieve efficiency comparable to that of the (expensive) isolation kits on the market.

2. Purity measurement of the extracted pDNA:

DNA purity was assessed by using the NanoDrop™ One Microvolume UV–Vis spectrophotometer, measuring the absorbance ratio of 260 and 280 nm wavelengths. A_{280} is measured to assess the presence of potentially contaminating proteins. Typically, pure DNA has an A_{260}/A_{280} ratio of 1.6 – 2.0 [42].

3. Agarose gel electrophoresis of the isolated pDNA:

We used a Mini-Sub Cell GT horizontal agarose gel electrophoresis system from Bio-Rad Laboratories (Hercules, CA, USA) to verify the success of the MNP-based DNA extraction. The procedure involved using agarose gels that were 0.75 cm thick with a concentration of 1.0 % (1 g of agarose powder dissolved in 100 mL of Tris-Acetate-EDTA buffer (TAE; 40 mM tris (hydroxymethyl) aminomethane, 20 mM acetic acid, 1 mM EDTA)) [43]. TAE solution also served as the running buffer for the electrophoresis. To ensure the sample had the necessary density for loading into the gel wells and to track the process, we used a 6× gel loading dye solution (comprising 1 part DNA loading dye and 5 parts isolated DNA sample), which contained 30 v/v % glycerol and 0.25 w/v % bromophenol blue dye [43]. The electrophoresis was conducted for 40 min at 90 V. Once separated with agarose gel electrophoresis, the resulting DNA fragments must be visible when exposed to ultraviolet (UV) light and must appear as clearly defined bands at the appropriate weight line determined by the DNA ladder [44].

4. Restriction digestion of the isolated pDNA:

The integrity and quality of the extracted DNA can be tested using restriction endonucleases, with specific recognition and cleavage sites on the pBAD24 plasmid molecule. These enzymes recognize a specific sequence on the DNA and (far from the recognition site) hydrolyze the phosphodiester bond between two neighbouring nucleotides in the DNA backbone [45]. The integrity of the DNA is confirmed if the enzyme activity results in the production of defined fragments. If the circular plasmid molecule has been broken or mutated at the recognition/cleavage site during the isolation process, the enzyme will not be able to recognize or bind and cut the sequence [46]. For these tests we used 1 μg of pDNA template, 1 U of FastDigest or conventional restriction enzyme(s) following the manufacturer's recommendation, and 2 μL of 10× buffer (FastDigest, Tango, Orange, Green or Red buffers) in a

final volume of 20 μL. Fast digestion with HindIII and VspI endonucleases was carried out for 10 min at 37 °C. The inactivation was done using a MultiTherm Shaker thermoblock (Benchmark Scientific, Edison, NJ, USA) at 65 °C for 10 min. Overnight digestions were performed in a Nuve EN 055 incubator (Nuve Laboratory & Sterilization Technology, Ankara, Turkey) at 37 °C, while the inactivation temperatures varied depending on the enzyme: for ClaI and VspI it was 65 °C for 20 min, and for HindIII it was 80 °C for 20 min.

5. qPCR of the extracted pDNA:

qPCR is most commonly used to detect gene expression, but it can also be employed to qualitatively [47] and quantitatively [48] measure DNA samples. In this research, we used qPCR for qualitative assessment to examine the integrity of the DNA molecules. If the DNA template is intact, the oligonucleotide primers hybridize to their complementary sequences at the appropriate temperature, and amplification of the sequence is achieved by DNA polymerase. The presence of the amplified product is indicated by the corresponding quantification cycle (Cq) value and fluorescence intensity. According to literature data, a Cq value of 35 corresponds to approximately 10 DNA copies, which is a very small amount. The lower the Cq value, the higher the DNA content of the initial sample [49]. On this basis, the criterion for qPCR was set at a Cq value below 35, with the fluorescence intensity evaluated by comparing it to that of the positive control sample, which is the same pBAD24 plasmid DNA sample, but isolated with a commercially-available extraction kit. This approach accounts for the fact that the relative fluorescence intensity units (RFU) depend not only on the amount of DNA amplified but also on the varying sensitivities of different instruments [50]. Therefore, it is not possible to define a specific range of RFU values that is universally acceptable. qPCR was performed with Azure Cielo™ Real-Time PCR (Azure Biosystems, Dublin, CA, USA). One well consisted of 5 ng DNA template, 1× Master Mix (DNA polymerase, $MgCl_2$, dNTPs (deoxynucleotide triphosphates), storage buffer) based on the manufacturer's recommendation, 0.4 μM forward primer, 0.4 μM reverse primer and 0.5× fluorescent PCR dye. PCR dye is a SYTO9 analogue with an excitation maximum of 485 nm and emission maximum of 498 nm. This can be excited with the SYBR/FAM channel of the qPCR instrument. In the qPCR reactions with pDNA templates, the ampicillin promoter forward and ampicillin reverse primers were used that are specific for the pBAD24 plasmid, while in the qPCR reactions with different gDNA templates, bacteria-specific primers were applied. The primer sequences and qPCR program can be found in *S2.3* of the *Supplementary Information*.

2.7. Bacterial transformation of the MNP-isolated pDNA samples

Three bacterial transformations were performed, one with each type (magnesium-, manganese- and nickel-containing ferrites) of the tested nanoparticles and each protocol (1, 2 and 3). *E. coli* JM109 Mix & Go! competent cells were used. 100 μL of competent cells were thawed on ice and transformed with 5 μL of pBAD24, an ampicillin resistance gene containing plasmid sample (*Table S2, SI*). Another tube of JM109 was transformed with pBAD24 sample isolated with a commercial MNP-based kit, serving as positive control of the experiment. 100 μL of the transformed cells were spread onto pre-warmed (37 °C) culture plate with 0.1 mg/mL ampicillin to see the selection. Plates were incubated at 37 °C for the colonies to grow. An inoculum from the agar plates was transferred into LB medium supplemented with ampicillin, to reconfirm plasmid selection and facilitate isolation of the pBAD24 from the overnight culture. Plasmid DNA was subsequently extracted using a commercial purification kit, and transformation of pBAD24 into competent cells was verified by agarose gel electrophoresis.

2.8. Isolation of pDNA from a complex biological matrix and gDNA from bacterial cell cultures with $MgFe_2O_4$-NH_2

5 mL of overnight cultured, pBAD24 containing *E. coli* cells were added to the same volume of blood serum with a mild contamination of red blood cells. After the mixture was vortexed and centrifuged, the isolation process was performed with amine functionalized magnesium ferrite and Protocol 1. Cultured cells were diluted and spread onto agar plates in a 10^6 dilution (100 μL) to calculate the CFU. The concentration and purity of the DNA isolates were assessed spectrophotometrically, and the samples were subsequently analyzed by agarose gel electrophoresis.

Extraction of genomic DNA from *Escherichia coli, Pseudomonas fluorescens, Micrococcus luteus* and *Bacillus subtilis* cells was performed based on the following protocol, developed in-house: 5 mL cell suspension was centrifuged (5 min, 6000×g) and the pellet was resuspended in 500 μL of buffer 1 (50 mM Tris–HCl pH 8.0, 50 mM EDTA pH 8.0, 0.5 % Tween 20) to which 0.2 mg/mL RNase A, 1.8 mg/mL lysozyme and 1.1 mg/mL proteinase K was added. Incubation in thermoblock at 37 °C lasted 30 min. Thereafter 175 μL of buffer 2 (3 M guanidine HCl, 20 v/v % Tween 20) was added to the sample. This was followed by incubation in thermoblock at 50 °C for 30 min. MNP dispersion in binding buffer (2.5 M NaCl, 10 mM Tris–HCl pH 4.0, 1 mM EDTA, 20 w/v % PEG 6000, 0.05 v/v % Tween 20) was prepared to a final MNP concentration of 10 mg/mL when added to the sample. The sample tube was rotated for 5 min at room temperature in a Mini Tube Rotator (Boekel Scientific, Feasterville-Trevose, PA, USA). After a few-minute incubation on the magnetic stand, the supernatant was removed. Washing of the MNP-DNA complex was conducted through adding the washing solution, vortexing and separating the pellet from the solution on the magnetic stand. This was performed in 3 steps: the first with 300 μL of 96 % ethanol and then twice with 300 μL of 80 % ethanol. The pellet was air dried in the incubator (37 °C, 15 min). 140 μL of 5 mM tris (hydroxymethyl) aminomethane (pH 10.0) was added to the dried pellet and the sample was incubated in a thermoblock shaker for 5 min, at 1400 rpm and room temperature. Separation of the gDNA containing elution fraction from the MNPs was performed on a magnetic stand and the DNA solution was separated to a new Eppendorf tube.

3. Results and discussion

3.1. Definition of criteria for evaluation of the results

Each pDNA isolation process utilizing one of the six MNPs and one of the three protocols was carried out at least three times for reproducibility. Based on the decision tree illustrated on Fig. 1, the determination was made regarding whether to proceed with each of the five specified evaluation procedures. For example, after the extraction step, DNA concentration and purity was measured. If these results were not acceptable based on the criteria described in section 2.6, additional testing on the isolate was not performed. If the purity and concentration of the DNA was acceptable, then we conducted agarose gel electrophoresis to further evaluate the quality of the pDNA. If electrophoresis results were favourable electrophoresis results, restriction digestion and qPCR were done to assess the integrity of the pDNA sample.

3.2. Overall performance of protocols and magnetic nanoparticles

A plasmid DNA isolation procedure using a specific protocol and MNP were deemed acceptable (indicated by a check mark in Table 3) if at least three parallel DNA extractions yielded satisfactory results. Cells marked with an X in Table 3 indicate that either the results of the procedure did not meet the required criteria or the procedure was not performed because of a previously failed outcome as outlined in the decision tree (Fig. 1). The last column of Table 3 provides a summary for each magnetic nanoparticle and for each protocol-nanoparticle pairing.

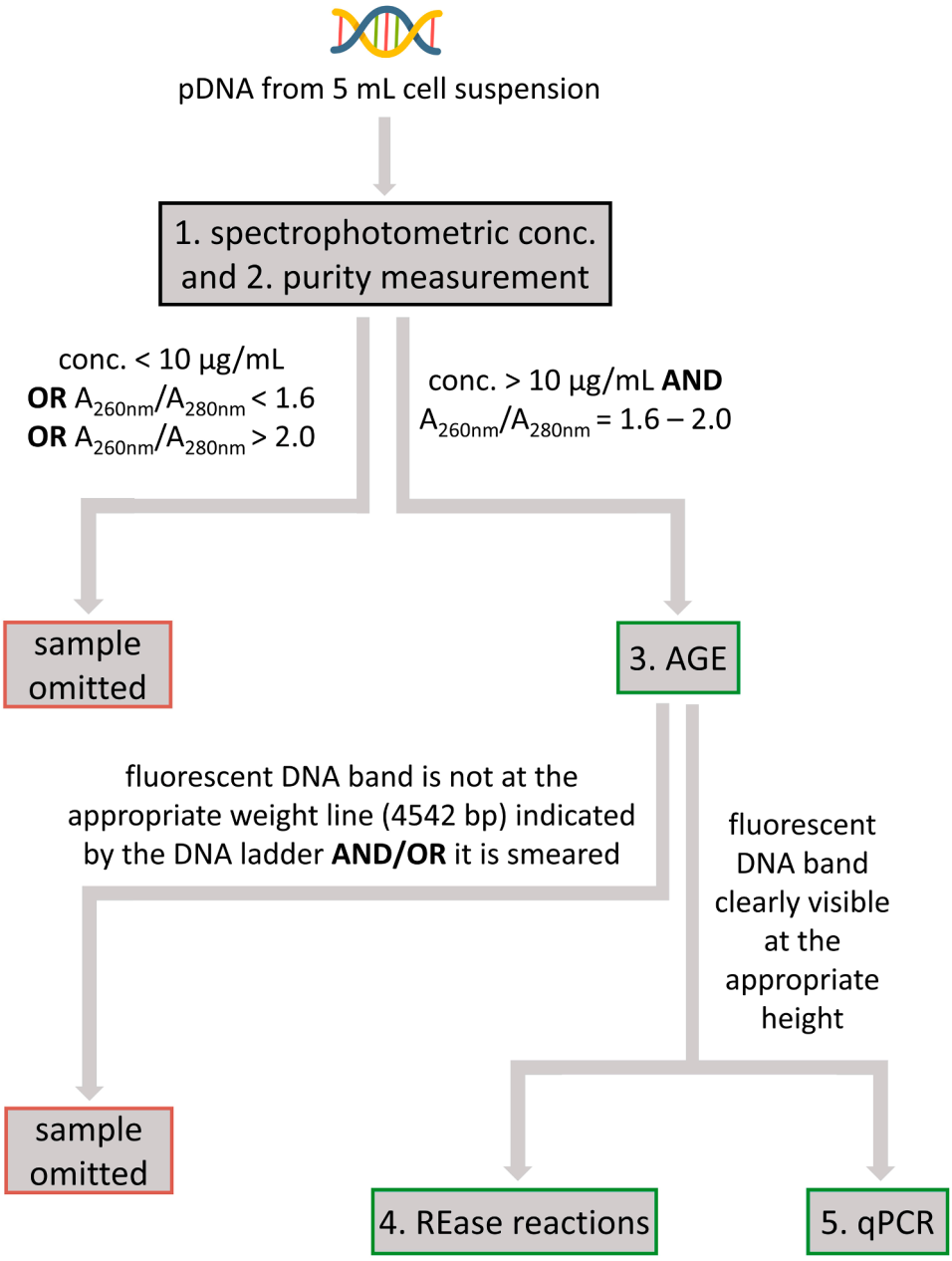

Fig. 1. Decision tree outlining the execution of the five evaluation steps performed after pDNA extraction. If the results met the criteria (shown next to the arrows), subsequent analysis were performed. Conc = concentration, AGE = agarose gel electrophoresis, REase = restriction endonuclease, qPCR = quantitative polymerase chain reaction.

Based on this summary, at least one protocol can be selected (indicated in green) for each MNP that can efficiently deliver high yields of high quality pDNA that can be utilized in downstream processes. For the $MnFe_2O_4$ MNP, Protocol 2 (NaCl-containing binding buffer, K-phosphate elution buffer) was found to be the most suitable. In contrast, Protocol 3 (no NaCl in the binding buffer, NaCl-containing elution buffer) yielded the best results for $MnFe_2O_4$-NH_2 and $NiFe_2O_4$ MNPs, while Protocol 1 (NaCl-containing binding buffer, Tris–HCl as elution buffer) was optimal for $NiFe_2O_4$-NH_2. Magnetic $MgFe_2O_4$ nanoparticles can be utilized with Protocols 2 and 3, while the $MgFe_2O_4$-NH_2 MNPs met the requirements for all three protocols, leading to the conclusion that this MNP is the most efficient for pDNA isolation among those tested.

3.3. Assessing the quantity and quality of extracted pDNA

After eliminating the specific MNP-protocol combinations that are not suitable for pDNA isolation, only those suitable for the extraction of pDNA of good quality and quantity were tested further. These include $MnFe_2O_4$ (with Protocol 2), $MnFe_2O_4$-NH_2 (Protocol 3), $NiFe_2O_4$ (Protocol 3), $NiFe_2O_4$-NH_2 (Protocol 1), $MgFe_2O_4$ (Protocols 2 and 3) and $MgFe_2O_4$-NH_2 (with Protocols 1, 2 and 3), which proved to be the most suitable for pDNA isolation, as it checked all the criteria for all three protocols.

Results of the concentration measurement carried out by UV–Vis spectrophotometer are shown in Fig. 2. The diagram illustrates the relative efficiency of the extraction carried out by each nanoparticle, highlighting with green and red those that had the highest ($MgFe_2O_4$ with Protocol 2) and lowest ($MnFe_2O_4$-NH_2 with Protocol 3) yields

Table 3
Summary of the pDNA isolation efficiency criteria based on subsection 2.6 (Conc. = Concentration, AGE = Agarose Gel Electrophoresis, REase = Restriction Endonuclease). Green colour indicates the protocols that met the criteria described in subsection 2.6.

DNA isolation with MNP	Protocol no.	Quantity	Quality		Integrity		Summary of the efficiency	
		Conc.	AGE	Purity	REase reaction	qPCR		
$MnFe_2O_4$	1	✓	✓	X	✓	✓	4/5	11/15
	2	✓	✓	✓	✓	✓	5/5	
	3	X	✓	X	X	✓	2/5	
$MnFe_2O_4$-NH_2	1	✓	✓	✓	X	✓	4/5	9/15
	2	X	X	X	X	X	0/5	
	3	✓	✓	✓	✓	✓	5/5	
$NiFe_2O_4$	1	✓	✓	✓	X	✓	4/5	9/15
	2	X	X	X	X	X	0/5	
	3	✓	✓	✓	✓	✓	5/5	
$NiFe_2O_4$-NH_2	1	✓	✓	✓	✓	✓	5/5	10/15
	2	X	X	X	X	X	0/5	
	3	✓	✓	✓	X	✓	4/5	
$MgFe_2O_4$	1	✓	✓	✓	X	✓	4/5	14/15
	2	✓	✓	✓	✓	✓	5/5	
	3	✓	✓	✓	✓	✓	5/5	
$MgFe_2O_4$-NH_2	1	✓	✓	✓	✓	✓	5/5	15/15
	2	✓	✓	✓	✓	✓	5/5	
	3	✓	✓	✓	✓	✓	5/5	

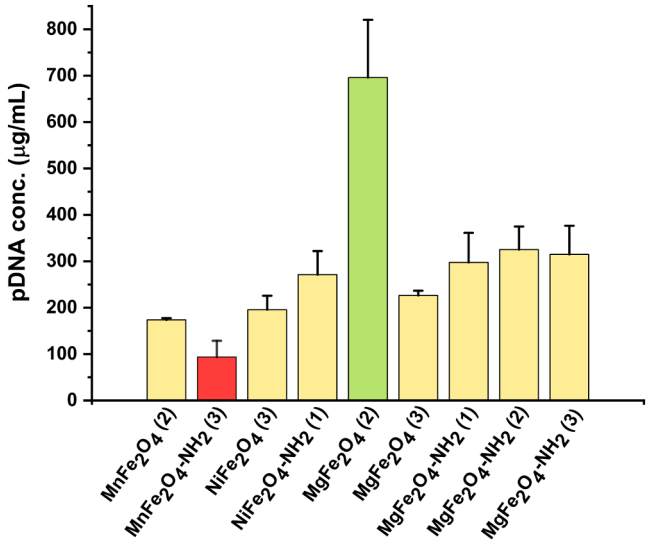

Fig. 2. Concentration of the MNP-isolated pDNA samples. X axis indicates the nanoparticle and protocol (no.) used for each isolation. The purity values (A_{260}/A_{280}) of the depicted pDNA samples fall within the expected range of 1.6 – 2.0.

(Fig. 2). Albeit the $MnFe_2O_4$-NH_2 MNPs yielded the least amount of pDNA (93.7 ± 35.2 µg/mL), this is still remarkably good result, as He et al. provided 55 µg/mL high copy plasmid pDNA with amino-modified magnetic nanoparticles [51]. Kruskal-Wallis H test was conducted to evaluate that there is significant difference in DNA concentrations, with the results presented in subsection *S3.4* of the *Supplementary Information*.

The overall charge of DNA molecules is negative due to the phosphate backbone, so they can adsorb to the surface of positively charged magnetic nanoparticles by electrostatic interactions. Amine-functionalized magnetic nanoparticles benefit from the increase in positive surface charge from -NH_2 groups on its surface that would result in enhanced DNA binding due to stronger electrostatic interactions [33]. However, this was observed only in case of nickel ferrite MNPs and in the case of magnesium ferrite (Fig. 2) under certain conditions ($MgFe_2O_4$ isolation with Protocol 3 compared to all three isolations with $MgFe_2O_4$-NH_2). The higher DNA yield obtained with the unmodified manganese ferrite can be attributed to its higher magnetic saturation (Ms) values (73 emu/g) compared to that of the amine-functionalized $MnFe_2O_4$ (37 emu/g) (*Figure S5, SI*) [52], which leads to an increase in the attractive forces between DNA and MNP. The difference in the quantity of the extracted pDNA with nickel ferrite MNPs can also be assigned to the higher magnetization of $NiFe_2O_4$-NH_2 (39 emu/g), than $NiFe_2O_4$ (26,7 emu/g) (*Figure S5, SI*) and to the smaller average crystallite size of the MNPs ($NiFe_2O_4$: 12 ± 3 nm, $NiFe_2O_4$-NH_2: 6 ± 2 nm) (*Figure S2, SI*), because smaller NPs have higher specific surface for the adsorption of molecules. DNA concentration values and therefore DNA quantity in the elution fraction determine the maximum adsorption capacity of the nanoparticles, which can be found in *Table S3, SI*.

The large difference in the amount of DNA extracted with magnesium ferrite nanoparticles under different conditions (isolations with Protocols 2 and 3) can be attributed to the varying conformations of DNA molecules in buffers at distinct salt concentrations. It is known that in aqueous solution the DNA molecule adopts an elongated structure due to the strong repulsion between the negatively charged phosphate groups [53,54]. For example, the length of a pDNA can be several hundred nanometers, while the diameter of a nanoparticle is at most 100 nm. Consequently, when pDNA molecules are mixed with MNPs, the free DNA wraps itself around the surface of the particle. One DNA molecule can occupy most of the surface binding sites of a single NP, but can also adsorb onto several other NPs due to its length and free anions along the

phosphate backbone [55]. As a result, the adsorption capacity of nanoparticles for DNA molecules is limited. However, when DNA is in a high salt concentration solution (such as 800 mM NaCl-containing buffer), it transitions from an elongated conformation to a more compact and dense globular structure [55,56]. In this state, some of the phosphate groups in the DNA backbone are shielded, reducing their availability for binding to positively charged nanoparticles. This means that only a portion of the phosphate groups in the globular molecules engage in electrostatic interactions, thereby decreasing the "footprint" each DNA molecule occupies on the surface of nanoparticles. This allows greater number of DNA molecules to adsorb onto each NP. The addition of a condensing agent (e.g. PEG) to the sodium chloride buffer further compresses the DNA molecules, enhancing their adsorption on the nanoparticle surface.

The lowest DNA yield was achieved with manganese ferrite nanoparticles and this can be attributed to the high aggregation capacity of the particles, that was observed by visualization during isolation procedures.

After UV–Vis spectrophotometry measurements, agarose gel electrophoresis was used to further evaluate the quality of the pDNA. Different bands are observed due to various conformations that pDNA can adopt (Fig. 3). These conformations have different migration patterns through the gel because of the structural differences, even though all have the same number of base pairs. For example the supercoiled (covalently-closed circular) pDNA is tightly closed, making it more compact, therefore able to travel quickly through the agarose gel (lower fluorescent bands in samples E1 and E2, Fig. 3). Plasmids can have multimeric forms (e.g. dimers, trimers), which appear higher up on the gel (higher fluorescent bands in samples E1 and E2, Fig. 3), as they are larger than monomeric forms. This phenomenon - resulting in slow migration - is attributed to recombination events or replication errors within the bacterial cell [57], rather than to DNA isolation errors.

In case of favourable results (distinct fluorescent DNA bands without smearing, Fig. 3), these samples were subjected to restriction digestion and qPCR to evaluate the integrity of the pDNA sample.

3.4. Assessing the integrity of the extracted pDNA

A reaction with the VspI specific restriction endonuclease was selected for the pDNA isolated with each of the nanoparticles. The VspI-digested samples are shown in Fig. 4 as a representative demonstration of integrity studies, involving restriction digestion with four different enzymes and two distinct activation intervals.

In the first column of the agarose gel the DNA ladder (Fig. 4) contains known sized DNA fragments and helps in the identification of the digested plasmids, which are located between the heights of the 4000 and 5000 bp marker bands. This leads to the conclusion that restriction digestion (linearization) was successful. The linear plasmid is another conformation of the molecule, less compact than the supercoiled form, which causes the molecule to migrate at a speed that is dependent on its size [57]. These results confirm that the pDNA extracted with nanoparticles and the aforementioned protocols is intact and of sufficient purity to be suitable for further molecular biological use.

qPCR was also used to demonstrate the suitability of pDNA samples in downstream processes. The quantification cycle (Cq) values of the samples, ranging from 8.32 to 15.74, indicate exceptional results (Fig. 5). First, all values are well below the threshold of 35 and near to that of the positive control (PC) value, as defined by the criteria in section 2.6. Additionally, the low Cq values suggest a substantial amount of the amplified product generated from the 5 ng of DNA used in each reaction. This demonstrates successful primer hybridization and efficient amplification by DNA polymerase, indicating a high-quality DNA template. The high Cq of the non-template control suggests that the primer dimers hybridized in the qPCR reaction, while the non-primer control has no amplification curve since the minimal amount of pDNA added to the reaction was not enough to generate a detectable fluorescent emission. The RFU values are presented in *Table S4*, and the statistical analysis assessing the significance of differences in Cq values is detailed in subsections *S2.5* and *S3.4* of the *Supplementary Information*.

The low Cq values obtained and the similarity of them suggest that the protocols optimized for the tested ferrite-based MNPs successfully yielded high-quality and amplifiable DNA. This reinforces the potential of these MNPs to serve as reliable alternatives in pDNA isolation, broadening the range of viable options for researchers.

3.5. Bacterial transformation of the MNP-isolated pDNA samples

Bacterial transformation was tested with an optimally functioning pDNA isolate for each magnetic nanoparticle: ($MgFe_2O_4$-NH_2 (Protocol 1), $MnFe_2O_4$ (Protocol 2), $NiFe_2O_4$ (Protocol 3)). Based on the ampicillin selection, all of the pBAD24 samples were successfully transformed into *E. coli* JM109 competent cells. From the transformed cells pBAD24 was isolated and run in agarose gel. The results reassured the success of the transformation. These findings suggest that neither the isolation conditions - specifically the composition of the elution buffer - nor the composition of the nanoparticles used for pDNA extraction adversely affected the transformation efficiency.

3.6. Results of pDNA isolated from bacteria-spiked blood serum and gDNA from bacterial cell culture using $MgFe_{2O4}$-NH_2 MNPs

As the most favourable results regarding pDNA extraction were obtained with the amine-functionalized magnesium ferrite, its effectiveness in isolating pDNA from a complex biological matrix and genomic DNA from different bacterial cells was further evaluated. From 5 mL of 1.57×10^9 CFU/mL bacterial cells we successfully isolated pDNA with concentrations of 303.1 μg/mL (first elution, E1) and 93.7 μg/mL (second elution, E2). The purity of the isolates as determined by A_{260}/A_{280} ratios, was 1.92 and 1.84, respectively. The agarose gel electrophoresis picture (Fig. 6) shows the pBAD24 molecules of the first and second elution fractions from the isolation.

Genomic DNA was extracted from both Gram-negative (*E. coli, P.*

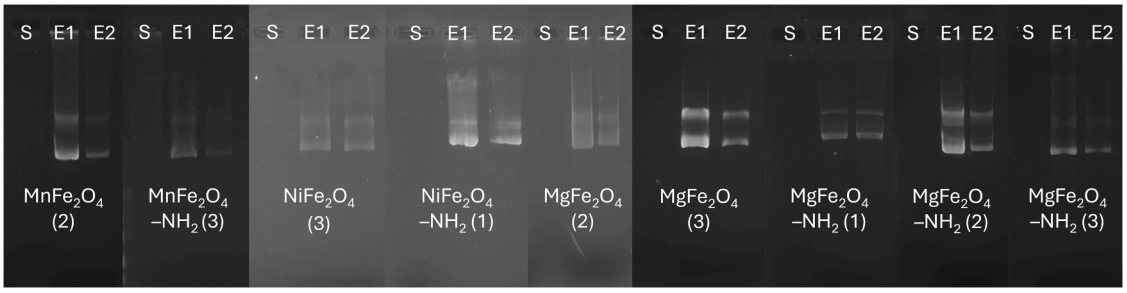

Fig. 3. Agarose gel electrophoresis picture of the isolated pDNA samples. *S* = supernatant (the fraction after the adsorption of DNA on MNPs), E1 = first elution fraction, E2 = second elution fraction.

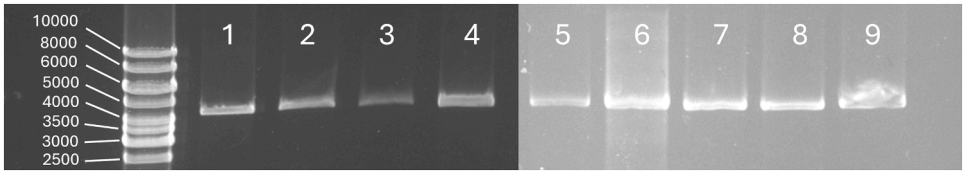

Fig. 4. VspI-digested pBAD24 samples isolated with the following MNPs (protocol no.): 1. $MnFe_2O_4$ (2), 2. $MnFe_2O_4$–NH_2 (3), 3. $NiFe_2O_4$ (3), 4. $NiFe_2O_4$–NH_2 (1) 5. $MgFe_2O_4$ (2), 6. $MgFe_2O_4$ (3), 7. $MgFe_2O_4$–NH_2 (1), 8. $MgFe_2O_4$–NH_2 (2), 9. $MgFe_2O_4$–NH_2 (3). The VspI enzyme has one cleavage site on the pBAD24 molecule, linearizing the circular plasmid, so that the fluorescent DNA band in the gel image is visible at the height corresponding to the actual size of the pBAD24 (4542 bp) DNA. The first (unnumbered) column shows the GeneRuler 1 kb DNA ladder from Thermo Scientific, numbers are displayed in bp (base pair).

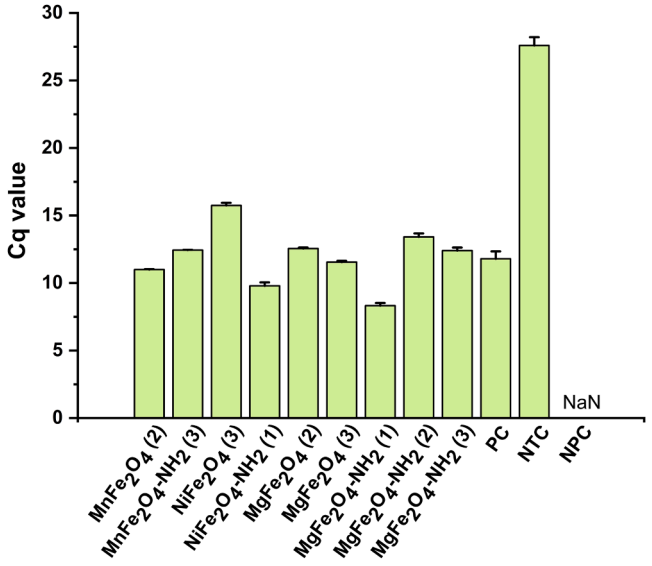

Fig. 5. qPCR reactions were performed with the pDNA templates isolated using the appropriate protocol for the specific MNP. The graph presents the mean of quantification cycle (Cq) values derived from triplicate measurements, along with the corresponding standard deviations. PC = Positive Control, NTC = Non-Template Control, NPC = Non-Primer Control, NaN = Not a Number.

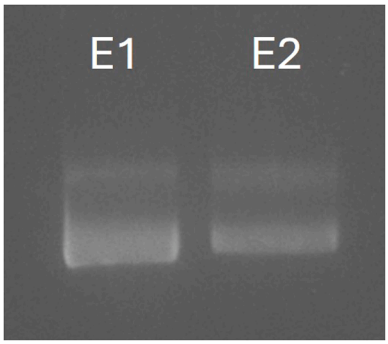

Fig. 6. Agarose gel electrophoresis picture of the pBAD24 pDNA isolated with $MgFe_2O_4$–NH_2 (Protocol 1) from a mixture of blood serum and bacterial cell culture (E1 = first elution, E2 = second elution).

fluorescens) and Gram-positive (*M. luteus, B. subtilis*) bacteria. The concentration and purity of the obtained samples are shown in Table 4 and Fig. 7, respectively.

The differences in gDNA concentration isolated with $MgFe_2O_4$-NH_2 from the Gram-negative and Gram-positive bacteria can be due to the different optical density (OD_{600}) values of the respective cell suspensions after an overnight incubation (growth) period. The OD measured at 600 nm wavelength of Gram-negative cells were higher (*E. coli* – 5.63, *P. fluorescens* – 6.08) than the values of Gram-positive cells (*M. luteus* – 4.5, *B. subtilis* – 3.9). Furthermore, the peptidoglycan layer in the membrane of Gram-negative bacteria is thinner than the membrane of Gram-positive bacteria, which decreases the efficiency of the chemical cell lysis of the latter [58], and this in turn affects the efficiency at which nucleic acids can be extracted. The gDNA purity is in the range defined by literature, even the A_{260}/A_{280} ratio value belonging to *E. coli* gDNA, because references say that only values appreciably lower than 1.6 show significant contamination of molecules that absorb strongly at or near 280 nm [59,60]. Similar studies have also tested iron oxide MNPs for gDNA isolation and their best yield from an *E. coli* strain was 18–20 μg/mL DNA [61], however the efficiency of our tested $MgFe_2O_4$-NH_2 obtained herein is almost 8 times better (154.5 μg/mL).

Table 4
Concentration and purity values of the $MgFe_2O_4$-NH_2 isolated gDNA samples.

Bacterium		MNP-isolated gDNA	
		concentration (μg/mL)	A_{260nm}/A_{280nm}
Escherichia coli	Gram-negative	154.5	1.57
Pseudomonas fluorescens		180.5	1.73
Micrococcus luteus	Gram-positive	77.9	1.63
Bacillus subtilis		83	1.65

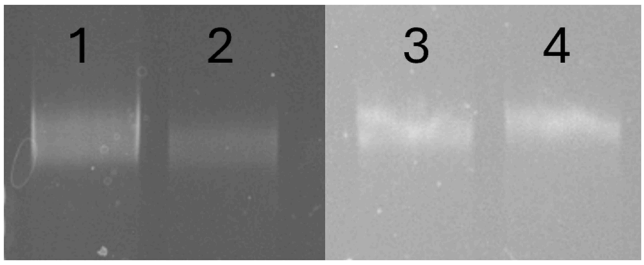

Fig. 7. Agarose gel electrophoresis pictures of gDNA isolated with $MgFe_2O_4$-NH_2 from Gram-negative and Gram-positive bacterial cells (1. *Escherichia coli*, 2. *Pseudomonas fluorescens*, 3. *Micrococcus luteus*, 4. *Bacillus subtilis*).

Agarose gel electrophoresis was carried out to ensure the presence of chromosomal DNA (Fig. 7). Distinct bands were observed for each sample, indicating the presence of high molecular weight genomic DNA with minimal fragmentation. The absence of significant smearing suggests that the DNA samples were not degraded during the isolation process. The successful application of the developed protocol to diverse bacterial types demonstrates its broad applicability and potential for further refinement to include other microbial species. Additionally, the efficiency observed here aligns with the results obtained for pDNA isolation, confirming the suitability of $MgFe_2O_4$-NH_2 for broader DNA isolation purposes across different biological contexts.

3.7. Integrity tests of the $MgFe_{2O4}$-NH_2-isolated gDNA in quantitative polymerase chain reactions (qPCR)

While DNA quantity and quality are typically evaluated using UV spectrophotometry, the integrity of a DNA sample can also be assessed with polymerase chain reactions [47]. The integrity tests should be carried out prior to large-scale extended genomic DNA experiments.

Each Cq value for the gDNA samples falls within the range of 22.66 and 26.29 (threshold was set to a maximum Cq of 35), indicating the amplification and thus the integrity of the templates (Fig. 8). Albeit the A_{260}/A_{280} ratio of the *E. coli* genome isolated with $MgFe_2O_4$-NH_2 MNPs was slightly out of the defined range of 1.6 – 2.0 with a value of 1.57, the qPCR results were satisfactory and comparable to the other gDNA samples with a purity value within the literature-accepted range [42]. This indicates that the minor contamination in the DNA sample does not impact the downstream applications of *E. coli* gDNA. *Table S5* in the *Supplementary Information* shows the RFU values of the measured samples.

This work highlights the potential of $MgFe_2O_4$-NH_2 MNPs as a reliable alternative to conventional DNA isolation techniques, many of which are labor-intensive or rely on toxic reagents. The ability to use MNPs for isolating gDNA from both Gram-positive and Gram-negative bacteria while maintaining compatibility with qPCR assays places this method among the advanced approaches for microbial genomic studies.

4. Conclusion

In this study we investigated the efficiency of ferrite-based magnetic nanoparticles for plasmid and genomic DNA isolation. Protocols were developed based on the quality and quantity of the extracted nucleic acid. Six magnetic nanoparticles were evaluated with 3 distinct extraction protocols, yielding a total of 18 experimental combinations. Among these, 9 combinations successfully met all defined quantitative (clearly visible fluorescent DNA bands in agarose gel electrophoresis, successful qPCR) and qualitative (UV–Vis spectrophotometry: pDNA concentration at least 10 μg/mL, A_{260}/A_{280} in the range of 1.6 - 2.0; successful restriction digestion) criteria, demonstrating their suitability for pDNA extraction: $MnFe_2O_4$ (Protocol 2), $MnFe_2O_4$-NH_2 (Protocol 3), $NiFe_2O_4$ (Protocol 3), $NiFe_2O_4$-NH_2 (Protocol 1), $MgFe_2O_4$ (Protocols 2 and 3), $MgFe_2O_4$-NH_2 (Protocols 1, 2 and 3). The best results were obtained with $MgFe_2O_4$ nanoparticles, which yielded the highest pDNA concentration (696 ± 124.4 μg/mL) with Protocol 2 (high salt concentration binding buffer, K_3PO_4 as elution buffer), while results with Protocol 3 (low salt concentration binding buffer, NaCl-containing elution buffer) were not as effective (226.2 ± 10.4 μg/mL). This can be explained with the different conformations of pDNA molecules in low and high salt concentration binding buffers. The lowest pDNA yield was achieved with the amine-functionalized manganese ferrite (93.7 ± 35.2 μg/mL, Protocol 3), however this concentration value can still be considered as high, compared to other iron oxide based MNP isolation protocols. Our findings indicate that while amine functionalization of MNPs does influence DNA extraction efficiency, magnetic saturation has a more pronounced effect.

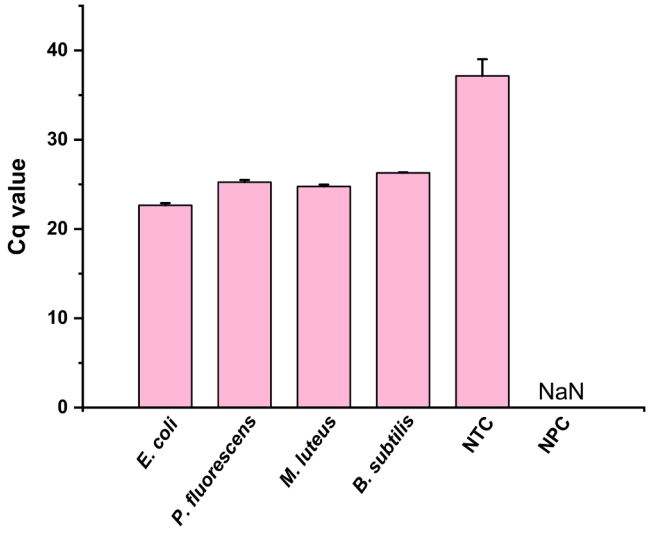

Fig. 8. qPCR reactions were performed with the gDNA templates isolated with MNP from each of the 4 mentioned bacterium species. The graph presents the mean of Cq values derived from triplicate measurements, along with the corresponding standard deviations. NTC = Non-Template Control, NPC = Non-Primer Control, NaN = Not a Number.

Based on the evaluation process, amine-functionalized magnesium ferrite was found to be the most versatile magnetic nanoparticle, as it is not protocol-sensitive and performing similarly under all three isolation conditions. For this reason, this nanoparticle is proposed for use, as it allows a wide range of applications for the extracted DNA. Therefore, it was tested to successfully isolate pure pDNA from bacteria-spiked blood serum and gDNA from four bacterial strains: *E. coli, P. fluorescens* (Gram-negative), *M. luteus, B. subtilis* (Gram-positive). Results of genomic DNA extraction were as valuable as we expected, however, the yields differ in the two types of bacteria. Isolation efficiency was higher in Gram-negative cells than in Gram-positive ones, which can be attributed to the varying OD values and the difference in thickness of the membranes of the two cell types, so the performed cell lysis may have had different efficiencies. Future investigations will focus on using MNPs to isolate nucleic acids from various biological sources, including fungi and plants. An additional objective is to refine the protocols established in this research using the tested nanoparticles for RNA isolation, thereby facilitating more efficient laboratory detection of various viral infections.

This article introduces two novel approaches: the use of nickel ferrite and amine-functionalized nickel ferrite MNPs as solid-phase tools for pDNA isolation, as well as the first application of amine-functionalized magnesium ferrite for gDNA extraction. The presence of amine groups on MNPs is advantageous not only due to their positive charge, which promotes strong electrostatic interactions with the negatively charged DNA during isolation, but also because this same interaction underlies their role in drug delivery systems. The amine–DNA binding contributes to preserving DNA integrity and enhances its stability in various biological media, making the DNA–MNP complexes biocompatible and suitable for a range of therapeutic applications [62,63]. Isolation of gDNA with the mentioned MNP is suitable for both Gram-negative and Gram-positive bacteria, and did so with a yield eight-times higher than those achieved with other MNPs. This research aims to identify a more efficient and cost-effective method of extracting of both plasmid and genomic DNA from cell cultures, while reducing the need for hazardous chemical exposure required by other approaches.

CRediT authorship contribution statement

Tímea B. Gerzsenyi: Writing – review & editing, Writing – original draft, Visualization, Methodology, Investigation, Formal analysis, Data curation, Conceptualization. **Ágnes M. Ilosvai:** Writing – review & editing, Writing – original draft, Resources, Methodology, Investigation. **Ferenc Kristály:** Methodology. **Lajos Daróczi:** Methodology. **Michael C. Owen:** Writing – review & editing, Writing – original draft, Validation. **Béla Viskolcz:** Funding acquisition. **László Vanyorek:** Writing – review & editing, Writing – original draft, Validation, Resources, Methodology, Investigation. **Emma Szőri-Dorogházi:** Writing – review & editing, Writing – original draft, Visualization, Validation, Supervision, Methodology, Investigation, Formal analysis, Data curation, Conceptualization.

Declaration of competing interest

The authors declare that they have no known competing financial interests or personal relationships that could have appeared to influence the work reported in this paper.

Funding

This work was supported by the EKÖP-KDP 2024 Cooperative Doctoral Program of the Ministry for Innovation and Technology from the source of the National Research, Development and Innovation Fund, Hungary.

Acknowledgements

This research could not have been performed without the following projects: TKP2021-NVA-14, 2020–1.1.6-JÖVŐ-2021–00009 (both funded by the Ministry for Innovation and Technology from the source of the National Research, Development and Innovation Fund, Hungary) and LIFE19 CCA/HU/001320 - LIFE-CLIMCOOP (funded by the European Union).

Supplementary materials

Supplementary material associated with this article can be found, in the online version, at doi:10.1016/j.btre.2025.e00904.

Data availability

Data will be made available on request.

References

[1] B. Rezaei, et al., Magnetic nanoparticles: a review on synthesis, characterization, functionalization, and biomedical applications, Small 20 (5) (2024) 2304848.
[2] S. Bandyopadhyay, H.C. Dorbala, S. Mandal, An overview of the impact of nanotechnology on economy and business, in: B. Sarkar, A. Sonawane (Eds.), An overview of the impact of nanotechnology on economy and business, Biological Applications of Nanoparticles (2023) 201–216. Editors.
[3] O.P. Fuentes, et al., Embracing sustainability in the industry: a study of environmental, economic, and exergetic performances in large-scale production of magnetite nanoparticles, ACS Sustain Chem Eng 12 (2) (2024) 760–772.
[4] L. Dong, et al., A review on recent advances in the applications of composite Fe3O4 magnetic nanoparticles in the food industry, Crit Rev Food Sci Nutr 64 (4) (2024) 1110–1138.
[5] A.I. Osman, et al., Synthesis of green nanoparticles for energy, biomedical, environmental, agricultural, and food applications: a review, Env. Chem Lett 22 (2) (2024) 841–887.
[6] W.-H. Huang, et al., Manganese ferrite modified agricultural waste-derived biochars for copper ions adsorption, Bioresour. Technol 367 (2023) 128303.
[7] X. Huang, et al., Nanotechnology in agriculture: manganese ferrite nanoparticles as a micronutrient fertilizer for wheat, Plants 13 (10) (2024) 1395.
[8] M.J. Uddin, Y.-K. Jeong, Adsorptive removal of pollutants from water using magnesium ferrite nanoadsorbent: a promising future material for water purification, Environ. Sci. Pollut. Res. 29 (7) (2022) 9422–9447.
[9] S. Debnath, R. Das, Strong adsorption of CV dye by Ni ferrite nanoparticles for waste water purification: fits well the pseudo second order kinetic and freundlich isotherm model, Ceram Int 49 (10) (2023) 16199–16215.
[10] A.R.O. Rodrigues, et al., Magnetic liposomes based on nickel ferrite nanoparticles for biomedical applications, Phys. Chem. Chem. Phys. 17 (27) (2015) 18011–18021.
[11] K. Asghar, M. Qasim, D. Das, Preparation and characterization of mesoporous magnetic MnFe2O4@ mSiO2 nanocomposite for drug delivery application, Mater. Today: Proc. 26 (2020) 87–93.
[12] F. Hyder, S.Manjura Hoque, Brain tumor diagnostics and therapeutics with superparamagnetic ferrite nanoparticles, Contrast Media Mol Imaging 2017 (1) (2017) 6387217.
[13] C.R. Kalaiselvan, N.D. Thorat, N.K. Sahu, Carboxylated PEG-functionalized MnFe2O4 nanocubes synthesized in a mixed solvent: morphology, magnetic properties, and biomedical applications, ACS omega 6 (8) (2021) 5266–5275.
[14] K. Islam, et al., Manganese ferrite nanoparticles (MnFe2O4): size dependence for hyperthermia and negative/positive contrast enhancement in MRI, Nanomaterials 10 (11) (2020) 2297.
[15] N. Alghamdi, et al., Structural, magnetic and toxicity studies of ferrite particles employed as contrast agents for magnetic resonance imaging thermometry, J Magn Magn Mater 497 (2020) 165981.
[16] N. Chaudhry, et al., Bio-inspired nanomaterials in agriculture and food: current status, foreseen applications and challenges, Microb, Pathog 123 (2018) 196–200.
[17] C. Ehi-Eromosele, et al., Synthesis and evaluation of the antimicrobial potentials of cobalt doped-and magnesium ferrite spinel nanoparticles, Bull Chem Soc Ethiop 32 (3) (2018) 451–458.
[18] S.D. Bharathi, D.R. Babu, Synthesis, characterization and antimicrobial activity of Manganese ferrite nanoparticles, Mater. Sci. Eng.: B 300 (2024) 117051.
[19] N. Lewinski, V. Colvin, R. Drezek, Cytotoxicity of nanoparticles, small 4 (1) (2008) 26–49.
[20] J. Nonkumwong, et al., Synthesis and cytotoxicity study of magnesium ferrite-gold core-shell nanoparticles, Mater. Sci. Eng.: C 61 (2016) 123–132.
[21] G.-f. Yang, et al., Preparation, characterization, in vivo and in vitro studies of arsenic trioxide Mg-Fe ferrite magnetic nanoparticles, Acta Pharmacol, Sin 30 (12) (2009) 1688–1693.
[22] S. Kanagesan, et al., Cytotoxic effect of nanocrystalline MgFe2O4 particles for cancer cure, J. Nanomater. 2013 (1) (2013) 865024.
[23] M.C. Symons, J.M. Gutteridge, Free Radicals and iron: chemistry, biology, and Medicine, Oxford University Press, 1998.
[24] N.L. Martínez-Rodríguez, S. Tavárez, Z.I. González-Sánchez, In vitro toxicity assessment of zinc and nickel ferrite nanoparticles in human erythrocytes and peripheral blood mononuclear cell, Toxicol. Vitro 57 (2019) 54–61.
[25] T.B. Gerzsenyi, et al., A simplified and efficient method for production of manganese ferrite magnetic nanoparticles and their application in DNA isolation, Int J Mol Sci 24 (3) (2023) 2156.
[26] J. Prodělalová, et al., Isolation of genomic DNA using magnetic cobalt ferrite and silica particles, J. Chromatogr. a 1056 (1–2) (2004) 43–48.
[27] J. Torres-Rodríguez, et al., Cobalt–zinc ferrite and magnetite SiO 2 nanocomposite powder for magnetic extraction of DNA, J Solgel Sci Technol 91 (2019) 33–43.
[28] S.C. Tan, B.C. Yiap, DNA, RNA, and protein extraction: the past and the present, Biomed Res Int 2009 (1) (2009) 574398.
[29] J.H. Min, et al., Isolation of DNA using magnetic nanoparticles coated with dimercaptosuccinic acid, Anal, Biochem 447 (2014) 114–118.
[30] C. Ma, et al., Magnetic nanoparticles-based extraction and verification of nucleic acids from different sources, J Biomed Nanotechnol 9 (4) (2013) 703–709.
[31] P. Oberacker, et al., Bio-on-Magnetic-beads (BOMB): open platform for high-throughput nucleic acid extraction and manipulation, PLoS Biol 17 (1) (2019) e3000107.
[32] S. Ehrt, D. Schnappinger, in: N. Casali, A. Preston (Eds.), Isolation of Plasmids from *E. Coli* By Alkaline Lysis, in *E. Coli* Plasmid Vectors: Methods and Applications, Humana Press, Totowa, NJ, 2003, pp. 75–78. Editors.
[33] Á.M. Ilosvai, et al., Simplified synthesis of the amine-functionalized magnesium ferrite magnetic nanoparticles and their application in DNA purification method, Int J Mol Sci 24 (18) (2023) 14190.
[34] K. Yasui, Numerical simulations for sonochemistry, Ultrason Sonochem 78 (2021) 105728.
[35] G.V. Mukamolova, et al., On resuscitation from the dormant state of Micrococcus luteus, Antonie Leeuwenhoek 73 (1998) 237–243.
[36] J. Errington, L.T.V. Aart, Microbe profile: bacillus subtilis: model organism for cellular development, and industrial workhorse, Microbiol. (Read.) 166 (5) (2020) 425–427.
[37] A.R. Tuttle, N.D. Trahan, M.S. Son, Growth and maintenance of *Escherichia coli* laboratory strains, Curr Protoc 1 (1) (2021) e20.
[38] G. Donnarumma, et al., Effect of temperature on the shift of Pseudomonas fluorescens from an environmental microorganism to a potential human pathogen, Int J Immunopathol Pharmacol 23 (1) (2010) 227–234.
[39] M. Samuel, et al., A spectrophotometric method to quantify linear DNA, Anal, Biochem 313 (2) (2003) 301–306.
[40] K.A. Boesenberg-Smith, M.M. Pessarakli, D.M. Wolk, Assessment of DNA yield and purity: an overlooked detail of PCR troubleshooting, Clin, Microbiol, Newsl 34 (1) (2012) 1–6.
[41] Mag-Bind®Ultra-pure plasmid DNA 96 kit. 26 July 2024]; Available from: https://omegabiotek.com/product/mag-bind-ultra-pure-plasmid-dna-kit/?cn-reloaded=1.
[42] G. Lucena-Aguilar, et al., DNA source selection for downstream applications based on DNA quality indicators analysis, Biopreserv Biobank 14 (4) (2016) 264–270.
[43] S. Surzycki, Basic Techniques in Molecular Biology, Springer Science & Business Media, 2012.
[44] P.Y. Lee, et al., Agarose gel electrophoresis for the separation of DNA fragments, JoVE (J. Vis. Exp.) (62) (2012) e3923.
[45] A. Pingoud, et al., Type II restriction endonucleases: structure and mechanism, Cell. mol. life sci. 62 (2005) 685–707.
[46] R.J. Roberts, K. Murray, Restriction endonuclease, CRC Crit, Rev, Biochem 4 (2) (1976) 123–164.
[47] S. Holdenrieder, et al., DNA integrity in plasma and serum of patients with malignant and benign diseases, Ann, N. Y. Acad, Sci 1137 (1) (2008) 162–170.
[48] J. Dang, et al., Development of a robust DNA quality and quantity assessment qPCR assay for targeted next-generation sequencing library preparation, Int, J. Oncol 49 (4) (2016) 1755–1765.
[49] A. Ruiz-Villalba, J.M. Ruijter, M.J. van den Hoff, Use and misuse of cq in qPCR data analysis and reporting, Life 11 (6) (2021) 496.
[50] P. Gill, Ø. Bleka, A.E. Fonneløp, Limitations of qPCR to estimate DNA quantity: an RFU method to facilitate inter-laboratory comparisons for activity level, and general applicability, Forensic Sci. Int.: Genet. 61 (2022) 102777.
[51] X. He, et al., Plasmid DNA isolation using amino-silica coated magnetic nanoparticles (ASMNPs), Talanta 73 (4) (2007) 764–769.

[52] D. Ang, et al., In vitro studies of magnetically enhanced transfection in COS-7 cells, Mater. Sci. Eng.: C 31 (7) (2011) 1445–1457.
[53] A. Savelyev, Do monovalent mobile ions affect DNA's flexibility at high salt content? Phys. Chem. Chem. Phys. 14 (7) (2012) 2250–2254.
[54] K. Yoshikawa, et al., Highly effective compaction of long duplex DNA induced by polyethylene glycol with pendant amino groups, J. Am, Chem, Soc 119 (28) (1997) 6473–6477.
[55] Z. Shan, et al., Promoting DNA loading on magnetic nanoparticles using a DNA condensation strategy, Colloids Surf. B: Biointerfaces 125 (2015) 247–254.
[56] T. Schlick, B. Li, W.K. Olson, The influence of salt on the structure and energetics of supercoiled DNA, Biophys, J 67 (6) (1994) 2146–2166.
[57] H. Birnboim, J. Doly, A rapid alkaline extraction procedure for screening recombinant plasmid DNA, Nucleic Acids Res 7 (6) (1979) 1513–1523.
[58] M. Mahalanabis, et al., Cell lysis and DNA extraction of gram-positive and gram-negative bacteria from whole blood in a disposable microfluidic chip, Lab Chip 9 (19) (2009) 2811–2817.
[59] G. Lucena-Aguilar, et al., DNA source selection for downstream applications based on DNA quality indicators analysis, Biopreserv Biobank 14 (4) (2016) 264–270.
[60] C. Mannu, et al., Comparison of different DNA extraction methods from peripheral blood cells: advice from the Fondazione Italiana Linfomi Minimal Residual Disease Network, Leuk. Lymphoma 57 (2) (2016) 400–410.
[61] A. Bandyopadhyay, S. Chatterjee, K. Sarkar, Rapid isolation of genomic DNA from *E. coli* XL1 blue strain approaching bare magnetic nanoparticles, Curr, Sci (2011) 210–214.
[62] A. Postigo, et al., Folding and functionalizing DNA origami: a versatile approach using a reactive polyamine, J. Am, Chem, Soc 147 (5) (2025) 3919–3924.
[63] M.I.S. Carlos, et al., Limiting the level of tertiary amines on polyamines leads to biocompatible nucleic acid vectors, Int J Pharm 526 (1–2) (2017) 106–124.